Interpretation of the Si $K\alpha$ x-ray spectra accompanying the stopping of swift Ca ions in low-density SiO_2 aerogel

J. Rzadkiewicz,[1,2] A. Gojska,[1] O. Rosmej,[3] M. Polasik,[4,*] and K. Słabkowska[4]
[1]*The Andrzej Soltan Institute for Nuclear Studies, PL-05-400 Świerk, Poland*
[2]*Institute of Plasma Physics and Laser Microfusion, Hery 23, PL-01-497 Warsaw, Poland*
[3]*Gesellschaft für Schwerionenforschung mbH, Plasma Physik, Darmstadt, Germany*
[4]*Faculty of Chemistry, Nicholas Copernicus University, PL-87-100 Toruń, Poland*
(Received 14 April 2010; published 9 July 2010)

This article presents a detailed analysis of the $K\alpha$ x-ray spectra of Si induced by 11.4 MeV/u Ca projectiles penetrating a low-density SiO_2 aerogel target measured with high spectral and spatial resolution at the UNILAC accelerator at GSI-Darmstadt. The low-density material used in the experiment was crucial for the space-resolved studies of the Si x-ray radiation (for different energies of stopping Ca ions). The stopping length of the 11 MeV/u Ca ions reaches up to 10 mm in the low-density SiO_2 aerogel, whereas in regular quartz solid targets it is about 100 times shorter. The analysis of the x-ray spectra emitted by the stopping medium has shown a high level of the L-shell ionization, especially in the later considered phase ($E_p \sim 5$ MeV/u) of the stopping process. It has been further demonstrated that the population of the highly ionized states produced in the ion-atom collisions can be substantially reduced in the time between the collision and the x-ray emission due to the very intense rearrangement processes occurring in Si situated in the chemical environment of oxygen atoms. Moreover, comparison of the experimental values of the $K\alpha$ L-shell satellite energy shifts with the results of the multiconfiguration Dirac-Fock calculations allows us to find that Si valence electron configuration is enriched due to electron transfer from valence-electron-rich oxygen atoms into highly ionized silicon atoms. Our results indicate that the Coulomb explosion in a highly ionized track core is prevented by rapid neutralization in the femtosecond time scale.

DOI: 10.1103/PhysRevA.82.012703 PACS number(s): 34.50.Fa, 32.30.Rj, 34.50.Bw, 32.70.Jz

I. INTRODUCTION

The radiative processes accompanying heavy-ion stopping in matter have been a subject of intensive studies in both experimental and theoretical physics. It was demonstrated that the K-shell radiation of projectile ions [1,2] and the stopping media [3–6] is a powerful diagnostic tool for investigating the charge-exchange processes occurring in ion-atom collisions. This knowledge is of great importance in many physical applications related to the determination of ion-stopping power [7], target radiation damage [8], development of techniques for material nanomodification [9], plasma generation by intense ion beams [10,11], and heavy-ion-based tumor therapies [12].

The processes occurring in the ion track core are also of fundamental interest to the development of the theory of the radiation damage processes [13–17]. The complex character of these phenomena is related to the local ion energy deposition, producing ionization of the stopping media in the nanometric vicinity of the projectile trajectory in the attosecond time scale. Due to the domination of the electronic stopping, the modification of the solid structures around the ion trajectory occurs indirectly, following the electronic excitation decay [13,14]. The relaxation of the primary electronic excitations of the target atoms caused by the heavy-ion Coulomb field is a complex phenomenon which splits into a sequence of events, sharply separated in the time scale ranging from subfemtoseconds to nanoseconds [14]. The features of the excited stopping material at the earlier stages of the radiation damage processes supply the initial conditions for the next kinetic stages. The femtosecond time scale of the primary electronic excitation makes the investigation of this early stage of the material modification difficult.

Ion-atom collisions lead to the charge-exchange processes between the projectile and the target atoms. Collisions with high-impact parameters cause ionization of the outer-shell electrons, while near-central collisions are mainly responsible for the production of the inner-shell vacancies in the target atoms. The inner-shell vacancy production gives rise to the x-ray radiation of both the moving ion and the target atom. This radiation depends greatly on the projectile velocity and its charge changing as the projectile penetrates the target. Therefore, the space-resolved x-ray spectra give fundamental information about the charge-exchange processes which occur along the ion beam stopping path and allow the determination of the projectile ion charge state evolution and ion track ionization degree. In addition, the Doppler shift provides a good separation of the x-ray spectra from the moving ions, enabling the determination of the ion velocity inside the interaction media [18–20].

The x-ray diagnostic of the ion-stopping process has clear advantages in comparison with the other methods. Since high-resolution x-ray measurements are charge-state specific, they give direct access to the charge-state distribution of the interacting ions inside the stopping media [20–23]. This is the most important advantage of the x-ray measurements not available for methods in which the ion charge-state distribution is determined when an ion escapes the target. The x-ray measurements with a spatial resolution along the ion beam stopping path give the information on the evolution of the heavy ion and the target radiation in coincidence with the ion penetration depth [18–21].

*mpolasik@uni.torun.pl

A typical lifetime of the K-shell vacancy state for the low-Z atoms is in a range of a few femtoseconds for highly ionized KL^N states (where N represents a number of the L-shell vacancies). Therefore, the K-shell radiation emitted from the interaction volume reflects the early stage after the excitation of the electronic subsystem in the heavy-ion track caused by the ion-atom collisions. For the x-ray transitions from the highly ionized KL^N states it is also possible to assess the influence of the atomic processes occurring in the time between the collision and the x-ray emission (Auger, Coster-Kronig, or interatomic transitions) on the structure of the K x-ray spectra. However, it should be mentioned here that in the case of highly ionized atoms being in the electron-rich chemical environment (e.g., SiO_2) this assessment can be difficult due to the extremely high intensity of the deexcitation processes, so-called cascading deexcitation [24]. Another advantage of this method is related to the fact that the K x-ray radiation requires a production of the K-shell vacancy in the ion-atom collision and therefore the investigations of the stopping processes are confined to the small impact parameters in the scale of the atomic L shell. Such quasi-impact-parameter-dependent experiments can be useful for testing the energy-loss theories [25].

Previous work investigated the way the projectile charge and its velocity evolved as the ion penetrated the target material [20]. The present article reports on the detailed analysis of the Si $K\alpha$ x-ray spectra induced by the decelerating Ca ions with initial energies of 11.4 MeV/u in the low-density SiO_2 aerogel. We focus on the problem of the primary electronic ionization or excitation of the stopping medium. In order to determine the initial distribution of the ionization degree in different phases of the stopping processes, we have studied the $K\alpha$ x-ray spectra of the ionized target atoms along the ion trajectory by means of the spectroscopic measurements with high spectral and spatial resolutions.

II. EXPERIMENT

The experiment was performed at the linear accelerator UNILAC at GSI in Darmstadt, Germany. The details of the experimental method and the setup were described in Refs. [18,20]. In the experiment the Ca ions with the initial charge $Z = +6$ and initial energy of 11.4 MeV/u were fully stopped inside the target placed in the vacuum chamber. The 0.2- to 0.5-μA pulsed ion beam was focused on the target. A 25-mm-thick porous, low-density SiO_2 aerogel was used as stopping target. The extremely low-density material ($\sim$0.023 g/cm^3) used in the experiment was crucial for the space-resolved studies of the x-ray radiation emitted in the stopping process. A very short stopping length of the fast heavy ions in regular quartz solid targets (the stopping length in quartz is not higher than 100 μm for $\sim$11 MeV/u Ca ions) makes a spatially resolved analysis of the K-shell radiation of the projectile and the target impossible.

A highly uniform porous material with colloidal microstructure consists of 3- to 5-nm solid SiO_2 beads forming a three-dimensional chain structure. The pockets between the beads are 30–50 nm, depending on the average density of the sample [26,27], and can be evacuated in the target chamber. It has been demonstrated experimentally that for a given porosity, projectile charge, and velocity [28], there is no remarkable influence of the porous nanostructure on the projectile and the target K-shell spectra. The comparison of the Si $K\alpha$ integrated spectrum obtained for porous (sum of the aerogel target spectra spatially resolved along the ion stopping path) and solid SiO_2 (unresolved spectrum of quartz due to the short ion stopping length) shows negligible differences [20].

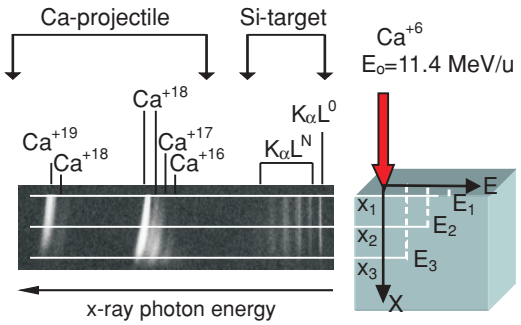

FIG. 1. (Color online) X-ray image representing Ca-projectile (tilted lines) and Si-target K-shell radiation registered simultaneously with a spatial resolution along the Ca-ion stopping path in SiO_2-gel target (0.02 g/cm^3). A symbol x represents the ion penetration depth while E is the average ion energy in a given phase of the stopping process.

The stopping length of the $\sim$11 MeV/u Ca ions in the low density SiO_2 aerogel reaches up to $\sim$10 mm and then the space-resolved analysis of the x-ray radiation induced in the different stages of the stopping processes becomes accessible (see Fig. 1). Another advantage of using aerogels is their high transparency for x-rays, which significantly reduces the absorption of $K\alpha$ photons emitted from the stopping medium. Therefore, one can observe the radiation emitted by the projectile and the stopping media directly from the interaction volume.

The $K\alpha$ x-ray spectra of the Ca projectiles and the stopping target were measured by means of x-ray spectroscopy using a focusing spectrometer with the spatial resolution (FSSR) based on a spherically bent crystal [26,27,29]. Such a spectrometer combines the Bragg reflection law with the spherical crystal-mirror configuration. In this way the high-energy resolution ($\Delta E \sim 0.4$ eV) on the one hand and high space resolution ($\Delta x \sim$ tens of μm) on the other hand are ensured. The angle between the ion beam and the direction in which the spatially resolved spectra were observed was 80°–90°. The reflected x-rays were recorded by using a direct-exposure x-ray film (DEF-5) that has high and stable sensitivity for the 1- to 10-keV photons [30]. An exposure time needed to record the high-quality space-resolved x-ray spectra was 2–5 h (for details, see Refs. [18–20]).

An image representing the space- and energy-resolved characteristic x-ray radiation emitted by the Ca projectile with initial energy of 11.4 MeV/u and the characteristic x-ray radiation of the ionized stopping media (Si) is shown in Fig. 1. The Ca-projectile spectra (3.2–3.9 keV) were registered by means of a spherically bent mica crystal in the fourth order of reflection and the Si $K\alpha$ spectra (1.7–1.9 keV) in the second one. The Doppler line shift of the projectile radiation which varies with the penetration depth due to the ion deceleration

was used to determine the ion velocities in the target. For details, see Refs. [18–20].

The spectra emitted by the stopping medium from the different stages of the stopping process consist of the $K\alpha L^0$ diagram and the $K\alpha L^N$ satellite lines. The $K\alpha L^0$ diagram lines correspond to $2p \rightarrow 1s$ transitions occurring in a single K-shell ionized atom. The $K\alpha L^N$ satellite lines originate from transitions in the atoms with a single K-shell hole and N holes in the L shell. The energies of the satellite transitions are higher than those of the ones in the diagram due to the reduced screening of the nuclear charge. The energy shifts of the $K\alpha L^N$ satellite transitions depend on the number of spectator holes in the L shell [31,32]. Since the energy shifts are relatively high (higher than the natural linewidth) due to each additional L-shell vacancy, the $K\alpha$ x-ray spectra can be resolved into the individual $K\alpha L^N$ satellite structures (see Fig. 1).

The energy shifts of the M-shell satellite lines corresponding to the different numbers of the M-shell holes are much smaller than those originating from the $K\alpha L^N$ satellite transitions. In the $K\alpha$ x-ray spectra the additional M-shell ionization is manifested as the broadening and the energy shifts of the $K\alpha L^N$ satellite structures. These additional shifts also depend on the number of the M-shell holes [33]. Therefore, the precise values of the Si $K\alpha L^N$ satellite energies give information on the M-shell valence configuration [32] that is crucial for the determination of the rearrangement processes occurring prior to the x-ray emission. This information is also of great importance for the diagnostics of the plasma nanostructures in the ion track.

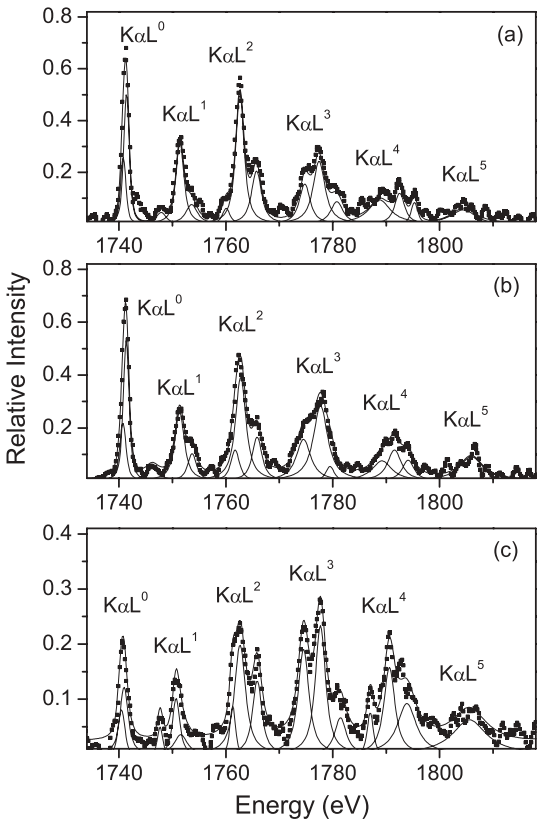

FIG. 2. High-resolution spectra of low-density SiO_2 aerogel induced by Ca projectiles for different penetration depths (and energies of the projectiles). (a) ~0.5 mm (11.4–10.6 MeV/u), (b) ~5 mm (8.5–7.6 MeV/u), and (c) ~10 mm (5.2–4.0 MeV/u). The results of the fitting procedure are also shown (solid lines).

III. DATA ANALYSIS

A. Fitting procedure

Using a scanning procedure, from the x-ray image (Fig. 1) we obtained three spectra which reflect the target radiation for the different values of the Ca-ion penetration depths inside the target and correspond to the different ion energies (see Fig. 2). The obtained spectrum corresponds to the $x_1 \sim$ 0.5-mm ion penetration depths and 11.4–10.6 MeV/u energies of the Ca projectiles. The successive spectra obtained in the scan correspond to the $x_2 \sim 5$ mm (8.5–7.6 MeV/u) and $x_3 \sim 10$ mm (5.2–4.0 MeV/u) of the ion penetration depths (projectile energies).

The space-resolved $K\alpha$ x-ray spectra were analyzed using the mean-square fit program. The line shape of the multiple ionized atoms reveals a very rich and complex structure due to different possible angular momentum coupling of the openlike subshells. In the case of Si, even the first-order $K\alpha L^1$ satellite line corresponding to the transitions occurring in the presence of one L-shell spectator vacancy consists of almost 2000 components [34]. The situation is further complicated by the fact that the M-shell configuration can be modified by the ionization and rearrangement processes, as well as by the chemical effects. Changes in the M-shell configuration can be additionally caused by the relaxation of excited states occurring in the plasma structures that appear in the ion track of the stopping media.

Since the energy differences of the components belonging to a given $K\alpha L^N$ satellite structure are smaller than the natural linewidths, all measured spectra can be decomposed into the well-resolved $K\alpha L^0$, $K\alpha L^1$, $K\alpha L^2$, etc., structures. In the fitting procedure all these structures were fitted by several Voigt profiles corresponding to the major multiplet components. Each Voigtian had the centroid energy and intensity as free parameters while the Lorentzian width was limited by the natural linewidths and the Gaussian width $\Gamma_G \sim 1$ eV (instrumental profile) was fixed. The limitation of the natural linewidth (0.48 eV) was set using the recommended values of the atomic level widths presented in Ref. [35]. Although these values refer to the single atomic systems, the corresponding widths for the Si chemical compounds are almost the same (the differences are not higher than 0.1 eV [36]). The background in all the spectra was represented by a linear function with a negative slope parameter in the range between -0.17 and -0.05 and a small positive constant correction (up to $\sim 10^{-4}$).

The results of the fitting procedure are presented together with the experimental spectra in Fig. 2. From the fitting procedure we obtained the average energy shifts of the Si $K\alpha L^N$ satellites and their relative intensities. The energy shifts were determined from the weighted average differences between centroids of the fitted Voigtians corresponding to the $K\alpha L^N$ satellites and the $K\alpha L^0$ diagram transitions. The $K\alpha L^N$ satellite intensities were obtained as a sum of the Voigtian areas representing the satellite structures.

B. MCDF calculations

The interpretation of the x-ray spectra emitted by Si being in a tetrahedral bond with oxygen requires molecular orbital calculations (e.g., see [37]). In our calculations, for the description of the K x-ray transitions we used a pure atomic model which accounts for the chemical (solid-state) effect by varying the electron valence configuration in the Si atomic system. Accordingly, in order to analyze the experimental $K\alpha L^N$ satellite spectra induced in the stopping processes, the transition energies and probabilities have been calculated by means of the multiconfiguration Dirac-Fock (MCDF) method [38]. The transverse (Breit) interaction and QED (self-energy and vacuum polarization) corrections were included in the calculations.

Within the MCDF method, the effective Hamiltonian for an N-electron system is expressed by

$$\hat{H} = \sum_{i=1}^{N} \hat{h}_D(i) + \sum_{j>i=1}^{N} \hat{C}_{ij}, \tag{1}$$

where $\hat{h}_D(i)$ is the Dirac operator for the ith electron. The terms $\hat{C}_{ij}$ account for the electron-electron interactions and are a sum of the Coulomb interaction operator and the transverse (Breit) operator. In the MCDF method, an atomic-state function describing the state s (with given values of the quantum numbers of the total angular momentum, J, and of its projection on the chosen direction, M, as well as the parity, p) is assumed in the multiconfigurational form

$$\Psi_s(JM^p) = \sum_m c_m(s)\Phi(\gamma_m JM^p), \tag{2}$$

where $\Phi(\gamma_m JM^p)$ are the configuration state functions (CSF), $c_m(s)$ are the configuration mixing coefficients for the state s, and γ_m represents all information required to uniquely define a certain CSF.

The MCDF calculations were performed for the diagram and the $K\alpha L^N$ satellite groups observed in the experiment ($K\alpha L^0$, $K\alpha L^1$, $K\alpha L^2$, ..., and $K\alpha L^5$). The $K\alpha L^N$ satellites correspond to the transitions occurring from the states having almost solely the $2p$ vacancies. The $2s$ holes are transferred into $2p$ subshell by the very intense Coster-Kronig transitions and the contribution of the $2s$ holes in the L-vacancy distribution at the moment of the K x-ray radiation can be neglected [39]. Therefore, in the MCDF calculations we used the following core vacancy configurations as the initial states: $1s^1 2s^0 2p^N$ ($N = 0,1,2,\ldots,$ and 5) for the $K\alpha L^0$, $K\alpha L^1$, $K\alpha L^2$, ..., and $K\alpha L^5$ transitions, respectively.

The symbol $K\alpha L^N$ in Table I concerns the energy shifts corresponding to the summary group, taking into account the statistically added $K\alpha L^N$ transitions from many initial $1s^1 2s^0 2p^N$ hole states. The M^4 label represents the fully ionized M shell. The M^0 configuration corresponds to the ground-state $3s^2 3p^2$ valence configuration (the free-atomic valence configuration).

The results of the calculations presented in the last column M^{chem} of Table I, attempt in a slightly simplified way (by using close subshell configurations) to take into account the valence charge fraction changed by the chemical effect. One should emphasize here that the chemical effect manifests itself in a completely different or even opposite way for the low- and high-ionized Si atoms placed in a chemical environment.

TABLE I. Theoretical $K\alpha L^N$ satellite energy shifts (in eV) for the different valence configurations (for details see text) with respect to the $K\alpha L^0$ diagram lines.

Satellite type	Valence configuration		
	M^4	M^0	M^{chem}
$K\alpha L^1$	16.8	11.9	10.2
$K\alpha L^2$	32.0	25.4	23.0
$K\alpha L^3$	48.8	40.4	37.3
$K\alpha L^4$	67.4	57.1	51.1
$K\alpha L^5$	88.0	75.8	68.0

The single K-shell ionized states (KL^0) of Si constitute the initial states of the $K\alpha L^0$ diagram transitions. In this case, the chemical effect decreases the number of the Si valence electrons by transferring them toward the oxygen neighbor atoms (the chemical bounding). The "chemical ionization" increases the energy of the $K\alpha L^0$ diagram transitions, causing a positive chemical shift. Because of the direct relationship between the effective valence charge and the energy shift, the latter is determined mainly by the electronegativity of the neighboring atoms [40]. The effective charge of Si in the SiO_2 compound was calculated by means of the discrete variational (DV) Hartree-Fock-Slater ($X\alpha$) method [41]. It was reported that in the SiO_2 compound, Si lost $\sim$1.4 electrons (transferred toward the oxygen atoms). We adopted this result in our x-ray energy calculations for the $K\alpha L^0$ diagram transitions. A linear combination of the $3s^1 3p^2$, $3s^2 3p^1$, and $3s^1 3p^1$ valence-shell configurations was used as the initial electron configuration (for details see [34]). The chemical shift of the $K\alpha L^0$ line relative to the corresponding one in a pure silicon atom was found to be $\Delta E_{\text{chem}} = 0.66$ eV [$E_{\text{chem}}(K\alpha L^0) = 1741.07$ eV], which is in very good agreement with the values 0.62 ± 0.01 [40] and 0.66 ± 0.01 [42] obtained in the experiments for the regular quartz and low-density SiO_2 aerogel, respectively. The measurements for low-density SiO_2 aerogel were performed at the Department of Physics, University of Fribourg (Switzerland), with the high-resolution von Hamos curved crystal spectrometer [43].

The transition energies of the $K\alpha L^N$ satellites originating from the highly ionized atoms should reveal a higher sensitivity to a chemical (solid-state) environment due to the reduction of the electronic screening. Therefore, one can naively expect an increase of the positive chemical shift in the case of the $K\alpha L^N$ satellite transitions. However, this uniform effective valence charge picture is valid only for the low-ionized states (KL^0) and breaks down in the case of the highly ionized states constituting the initial state configuration for the $K\alpha L^N$ satellite transitions. After creation of many L-shell vacancies in Si, the valence electrons of the SiO_2 compound, which are initially distributed near to the electronegative oxygen ligands, are rapidly rearranged toward the Si positive field center [24]. Moreover, a high inner-shell ionization enhances the binding potential to such an extent that the valence shell configuration is completed according to the free atomic structure principle. As a result, the valence shell of the highly ionized Si atoms

after the interatomic relaxation is significantly enriched with electrons. Therefore, contrary to the low-ionized states, the chemical effect reduces energies of the high-order $K\alpha L^N$ satellite transitions, causing a negative chemical shift. This effect greatly depends on a number of the L-shell vacancies. In order to introduce this effect in the quantitative way, we calculated the energy shifts with the mutable valence-shell configurations, the $3s^2 3p^4$ and $3s^2 3p^6$ for the $K\alpha L^{1,2,3}$ and $K\alpha L^{4,5}$ satellite transitions, respectively.

The chemical enrichment effect competes with other processes which can also modify the valence-shell structure, for example, dense nanoplasma effects [44–46]. Therefore, a detailed analysis of the $K\alpha L^N$ satellite energy shifts brings unique information on the valence-shell configuration that is crucial not only for the determination of the L-shell rearrangement intensities but also for a reliable framework for the ion track plasma modeling.

C. Primary vacancy distributions accompanying the stopping processes

The intensity of the K-shell radiation strongly depends on the inner-shell vacancy production. The K-shell ionization occurs effectively in ion-atom collisions with close to zero impact parameters. Figure 3 represents cross-sections of the K-shell vacancy production in Si atom ionized by a Ca projectile depending on the ion energy and charge. In the Ca-ion energy range of 2–10 MeV/u the cross sections calculated by means of the Loss code [22] are relatively high and change from 5×10^{-18} to 7×10^{-18} cm^2. At the lower projectile energies the production of the Si K-shell vacancies is not effective any more and the K-shell radiation can hardly be observed.

The values of the cross sections for the K-shell ionization of Si by the Ca ions allow us to estimate the mean free path of the Ca ions for the Si K-shell vacancy production as $l_K = 1/\sigma_K n_a$, where σ_K is a cross section for the K-shell ionization (in cm^2) and n_a is a density of the target atoms (in cm^{-3}). From the comparison of the K-shell ionization free path ($l_K \sim$ 20–40 nm) with the interatomic distance of 0.23–0.3 nm between the Si atoms in quartz, one can estimate that every 100th Si atom undergoes the K-shell ionization. The production of

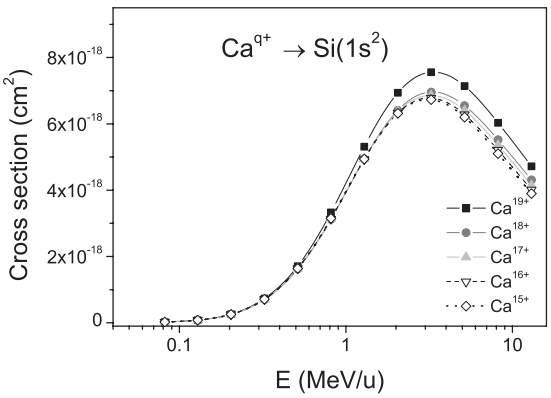

FIG. 3. Theoretical K-shell ionization cross sections (Loss code [22]) for Si target atoms bombarded by Ca^{q+} ions (q = 15–19) plotted as a function of the projectile energy.

the K-shell vacancy in a single ion-atom collision can be accompanied by the L- and M-shell ionization. In this way, the Si target atom can reach a very high degree of ionization. The same estimations made for the M ($l_M \sim$0.2–0.5 nm)- and L-shell ionization free paths ($l_L \sim$2–6 nm) indicate that almost every Si atom around the ion trajectory is M-shell ionized and every 10th atom is L-shell ionized. This leads to the extremely inhomogeneous distribution of the ionization degree of the target media along the ion path directly after the ion-atom collision and consequently to a complex structure of the target x-ray spectrum.

The Monte-Carlo calculations performed for the Si target ionization by 11.4 MeV/u Ca ions [47] showed that the energy of about 60% ionized electrons is in the range of 10–100 eV. This slow electron fraction cannot escape the track core due to the strong Coulomb potential produced by the ionized atoms. Another, highly energetic electron fraction escapes the interaction region and causes the K-shell ionization of the unperturbed atoms far away from the ion track. That is why the diagram $K\alpha$ lines observed in the experiment have much higher intensities than those expected from the direct ion-atom interaction.

A degree of the projectile track ionization and the amount of the slow and fast electrons determine the succeeding processes occurring in the track. At least two different scenarios are possible. First, if the ion track is strongly ionized and the core neutralization does not occur during the first tens of femtoseconds, the repulsion of the highly ionized target atoms can lead to the Coulomb explosion [15,16] and to the deformation of the crystal structure around the ion track. As opposed to that, the Coulomb explosion can be prevented if the ion track is weakly ionized and/or if a fast neutralization occurs due to the return of ionized slow electrons. Partially, the information on the fast electron fractions can be obtained from the enhanced intensities of the diagram $K\alpha$ transitions. In order to study the degree of the track ionization in the nearest vicinity of the Si atoms, one can use a statistical approach presented in what follows.

In the case of the direct ionization occurring in the near-central collision, the L-shell electrons are mainly ejected in an uncorrelated way (the direct Coulomb ionization) and one can therefore expect a binomial distribution of the KL^N states population. The validity of this approximation has been confirmed in many previous works [48,49]. The cross section for the production of the KL^N state can be written in the independent electron approximation as

$$\sigma_{KL^N} = 2\pi \int_0^\infty 2p_K(b)[1 - p_K(b)] \times \binom{8}{N} p_L^N(b)[1 - p_L(b)]^{8-N} b db, \qquad (3)$$

where p_K and p_L are the mean K- and L-shell ionization probabilities (per electron), respectively. The values of the ionization probabilities as a function of the impact parameter can be obtained from the semiclassical approximation (SCA) calculations [50,51]. The model describes an ion-atom collision using the first-order time-dependent perturbation theory. This theory was used in the description of the K- [52], L- [39], and M-shell [33] ionization processes. In the case of

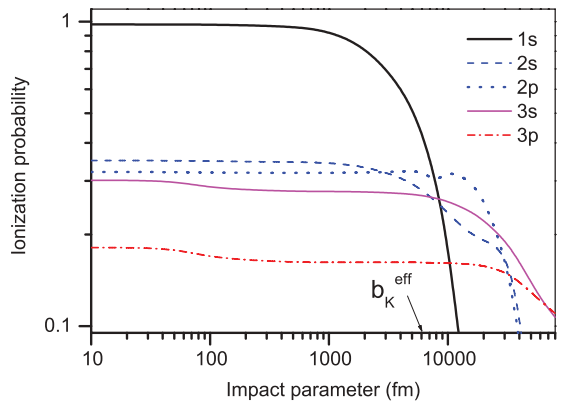

FIG. 4. (Color online) Theoretical SCA ionization probabilities of K, L, and M (sub)shells as functions of the impact parameter of Si atoms bombarded by 11 MeV/u Ca ions.

low-Z atoms, it was found that the SCA theory with hydrogenlike wave functions (SCA-HYD) calculations provide a reasonable description of the L-shell ionization caused by heavy ions ($Z_P \sim 6$–10) in the high-velocity regime ($v/v_L > 1.5$) [39].

Figure 4 shows the K-, L- and M-subshell ionization probabilities calculated by means of the SCA-HYD in a separated-atom (SA) mode. The L-subshell ionization probabilities remain stable for a relatively long range of the impact parameter values. By introducing the $b^{\text{eff}} = 6000$ fm value for which the product $b \times p_K(b)$ reaches the maximum, in the low-impact parameter region ($0 \leqslant b \leqslant b^{\text{eff}}$) it is possible to describe the L-shell vacancy distribution by a single (constant) parameter $p_L(b^{\text{eff}})$. This simplifies Eq. (3) into the formula

$$\sigma_{KL^N} = \binom{8}{N} p_L^N(b^{\text{eff}})[1 - p_L(b^{\text{eff}})]^{8-N}\sigma_K, \qquad (4)$$

where σ_K is the total cross section for the K-shell vacancy production. It should be pointed out here that besides the direct K-shell ionization also electron-capture processes can contribute to the K-shell vacancy production [53].

The binomial distribution of the target atom L-shell vacancies can be modified by the electron capture from the target atom into a projectile [39,54]. Therefore, the statistical model describing the primary vacancy distributions of the Si KL^N states produced in the stopping processes should also take into consideration the electron-capture processes occurring in the near-central collisions. The total cross sections for the L-shell vacancy production by the electron capture from Si into Ca ions can be calculated by means of the nonrelativistic eikonal theory [55]. The results of these calculations for different ion penetration depths (and ion energies) are shown in Table II. Assuming that the capture to ionization cross section ratios are similar to the ratios of the corresponding probabilities for central collisions, one can estimate the capture probabilities for small impact parameters.

The results in Table II indicate that the L-K electron-capture process is very weak (more than three orders of magnitude weaker than the direct L-shell ionization) and does not play an important role in the production of the L-shell vacancies in any stage of the stopping processes. This role is further reduced by the fact that the charge-state fraction of the

TABLE II. Theoretical cross sections for L-electron capture (eikonal approximation [55]) and direct ionization (SCA approximation) of Si atoms by fully stripped Ca ions in cm^2.

Projectile energy	$\sigma^{\text{EC}}_{L\to K}$	$\sigma^{\text{EC}}_{L\to L,M}$	σ^{DI}_{L}
11 MeV/u	8.1×10^{-20}	2.0×10^{-19}	2.9×10^{-17}
8 MeV/u	7.1×10^{-21}	7.7×10^{-19}	4.1×10^{-17}
5 MeV/u	4.6×10^{-21}	6.6×10^{-18}	6.5×10^{-17}

Ca ions with the energy of a few MeV/u colliding with SiO_2 is dominated by Ca^{18+} and Ca^{17+} ions [20], which makes the electron capture into the K-shell hardly possible.

Due to the negligible contribution of the L-K electron capture, in our analysis we took into consideration only the L-L and L-M electron-capture processes:

$$p_L^{\text{EC}} \approx p^{\text{EC}}_{L\to L} + p^{\text{EC}}_{L\to M}. \qquad (5)$$

Assuming that L-shell vacancies can be produced independently in the direct ionization and/or in the electron-capture processes, both partial L-shell vacancy distributions related to the direct ionization and electron-capture processes can be described by binomial distributions. The relative population of n vacancies from l L-shell electrons produced in direct ionization processes can be written as follows:

$$P^{\text{DI}}_{(n,l)} = \binom{l}{n} \left(p_L^{\text{DI}}\right)^n \left(1 - p_L^{\text{DI}}\right)^{l-n}, \qquad (6)$$

where p_L^{DI} represents the L-shell direct ionization probability per electron. The relative population of n' vacancies from l' L-shell electrons produced in the L-L and L-M electron-capture processes can be written in a similar way:

$$P^{\text{EC}}_{(n',l')} = \binom{l'}{n'} \left(p_L^{\text{EC}}\right)^{n'} \left(1 - p_L^{\text{EC}}\right)^{l'-n'}, \qquad (7)$$

where p_L^{EC} is the total electron-capture probability per electron.

It was further assumed that the L-shell production is a two-step process related to the following ionization and/or electron capture (or vice versa). Such an approach gives the following distribution model for the population of the KL^N states:

$$\begin{aligned} P_L^N = {} & \tfrac{1}{2}\left[P^{\text{EC}}_{(0,8)}P^{\text{DI}}_{(N,8)} + P^{\text{EC}}_{(1,8)}P^{\text{DI}}_{(N-1,7)} + P^{\text{EC}}_{(2,8)}P^{\text{DI}}_{(N-2,6)}\right. \\ & \left. + P^{\text{EC}}_{(3,8)}P^{\text{DI}}_{(N-3,5)} + \cdots + P^{\text{EC}}_{(N,8)}P^{\text{DI}}_{(0,8-N)}\right] \\ & + \tfrac{1}{2}\left[P^{\text{DI}}_{(0,8)}P^{\text{EC}}_{(N,8)} + P^{\text{DI}}_{(1,8)}P^{\text{EC}}_{(N-1,7)} + P^{\text{DI}}_{(2,8)}P^{\text{EC}}_{(N-2,6)}\right. \\ & \left. + P^{\text{DI}}_{(3,8)}P^{\text{EC}}_{(N-3,5)} + \cdots + P^{\text{DI}}_{(N,8)}P^{\text{EC}}_{(0,8-N)}\right], \end{aligned} \qquad (8)$$

where $P^{\text{DI}}_{(n,l)}$ and $P^{\text{EC}}_{(n'l')}$ correspond to the partial L-shell vacancy populations obtained from binomial distributions and $N = n + n'$ represents the total number of the L-shell vacancies produced in both the direct ionization and the electron-capture processes, respectively. A similar approach is presented for the L-shell ionization and the L-K electron-capture processes in Refs. [39,54].

Using this model and employing the fitting procedure, one can obtain the primary L-shell vacancy distributions within errors. In order to obtain unambiguous results from the fitting procedure, only one free parameter has to be

used (the ionization and electron-capture processes cannot be distinguished in a statistical model). Since the direct L-shell ionization significantly dominates over the L-shell electron capture at high projectile energies, we fixed the electron-capture probabilities by taking estimated values from the theory, while the ionization probabilities were used as free parameters. In this way we obtained the primary L-shell vacancy distributions and the L-shell ionization probabilities for all considered stages of the stopping process.

Further modification of the KL^N states distribution can be caused by fast electrons and x-ray secondary ionization [56,57]. This enhances the $K\alpha L^0$ diagram lines observed in the x-ray spectra. However, since this process is not related to the direct ion-atom interaction, the $K\alpha L^0$ lines have been excluded from the analysis of the primary vacancy distributions.

The interpretation of the $K\alpha L^N$ satellite intensities also requires taking into account the L-shell rearrangement transitions and changes in fluorescence yields due to the additional ionization. Significant changes of the M-shell electron population followed by the intense rearrangement processes lead to the filling of the L-shell (and K-shell) vacancies in the ionized Si. The role of the valence electrons or chemical bounding in the rearrangement processes which occur after the initial electronic excitation [24,58–62] is presented in the next section.

D. Rearrangement processes

The $K\alpha L^N$ satellite intensities observed in the experiment reflect the L-shell vacancy fraction in the stopping media at the moment of the $K\alpha$ x-ray emission. Determination of the primary L-shell vacancy distribution (at the moment of the projectile-target interaction) requires the calculations of rearrangement probabilities in all the processes that modify the number of the L-shell vacancies during the time between the collision and the photon emission (lifetimes of KL^N states increase in Si from ~1.5 fs for $N=0$ to ~tens of fs for $N=8$).

The X^N diagram ($N=0$) and the satellite ($N=1,2,\ldots$) intensities of the $K\alpha L^N$ transitions observed in the x-ray spectra are related to the primary vacancy yields I^N by the following equations:

$$X^0 = (I^0 + R_1 I^1 + R_1 R_2 I^2 + \cdots + R_1 R_2, \ldots, R_8 I^8)\omega^0_{K\alpha}, \tag{9a}$$

$$X^N = (I^N + R_{N+1} I^{N+1} + \cdots + R_{N+1}, \ldots, R_8 I^8) \times (1 - R_N)\omega^N_{K\alpha}, \tag{9b}$$

$$X^8 = I^8(1 - R_8)\omega^8_{K\alpha}, \tag{9c}$$

where $R_1, \ldots, R_{N+7}$ are the probabilities of an electron rearrangement for a given L-shell hole configuration. The $\omega^N_{K\alpha}$ factors represent the partial fluorescence yields of the $K\alpha$ transitions with the N number of L-shell spectator vacancies:

$$\omega^N_{K\alpha} = \frac{\Gamma^{\mathrm{R}}_{K\alpha}(L^N)}{\Gamma^{\mathrm{R}}_{K\alpha}(L^N) + \Gamma^{\mathrm{R}}_{K\beta}(L^N) + \Gamma^{\mathrm{A}}_{K}(L^N)}, \tag{10}$$

where $\Gamma^{\mathrm{R}}_{K\alpha}(L^N)$ and $\Gamma^{\mathrm{R}}_{K\beta}(L^N)$ are the radiative widths of the $K\alpha$ and $K\beta$ transitions, while $\Gamma^{\mathrm{A}}_{K}(L^N)$ widths correspond to the K-shell Auger transitions in the presence of the N number of L-shell spectator vacancies, respectively. By taking into consideration the LMM Auger and radiative $M \to L$ transitions which reduce the number of L-shell holes produced in the ion-atom collisions one can find rearrangement probabilities. Therefore, the probability that an L-shell vacancy will be filled within the lifetime of a K-shell hole is given by

$$R_i = \frac{\Gamma^{\mathrm{A}}_{L_i} + \Gamma^{\mathrm{R}}_{L_i}}{\Gamma_K + \Gamma_{L_i}}, \tag{11}$$

where Γ_K and $\Gamma_{L_i} = \Gamma^{\mathrm{A}}_{L_i} + \Gamma^{\mathrm{R}}_{L_i} + \Gamma^{\mathrm{CK}}_{L_i}$ are the total widths of the K and L_i atomic levels, while $\Gamma^{\mathrm{A}}_{L_i}$, $\Gamma^{\mathrm{R}}_{L_i}$, $\Gamma^{\mathrm{CK}}_{L_i}$ represent the partial widths for the Auger, radiative, and Coster-Kronig transitions, respectively. In the case of the Si atom, any L_1 subshell holes are immediately transferred into the L_2 or L_3 subshells *via* the Coser-Kronig transitions ($p^{\mathrm{CK}}_{L_1 \to L_{23}} \approx 98\%$ [63]).

Therefore, Eq. (11) can be reduced to the form

$$R \approx R_{23} = \frac{\Gamma^{\mathrm{A}}_{L_{23}} + \Gamma^{\mathrm{R}}_{L_{23}}}{\Gamma_K + \Gamma_{L_{23}}}. \tag{12}$$

For singly ionized atoms, as the K-shell partial widths, we used values taken from Refs. [64] ($\Gamma^{\mathrm{R}}_{K\alpha}$ and $\Gamma^{\mathrm{R}}_{K\beta}$), [65] ($\Gamma^{\mathrm{A}}_{KLL}$, $\Gamma^{\mathrm{A}}_{KLM}$), and [66] ($\Gamma^{\mathrm{A}}_{KMM}$) for the radiative and Auger transitions, respectively. In the case of the L_{23} subshells, the widths of the radiative $M \to L_{23}$ and Auger $L_{23}MM$ transitions were taken from Ref. [63].

The estimated rearrangement factors presented earlier can only be used for the single L-shell ionized atoms. In the case of the multiply ionized atoms, one should take into consideration the changes of the widths (transition rates) appearing in Eq. (12). The rates of the rearrangement transition occurring in the time between the ion-atom collision and the $K\alpha$ x-ray emission greatly depend on the Si valence charge fraction. This fraction is governed by the M-shell ionization and the chemical environment of Si. In addition, the low-temperature plasma structure appearing locally as a result of the target heating can influence the valence vacancy configuration. In Table III the rearrangement probabilities obtained by means of the atomic local-potential model with the extended scattered-wave integration technique [24] are presented for various

TABLE III. Theoretical values of rearrangement probabilities R_N for KL^N states of Si in different valence configurations (M^4, M^0, M^{chem}). The M^{scal} values correspond to the rearrangement probabilities obtained by means of scaling procedure (for details see Refs. [54,67]).

Rearrangement factor	Valence configuration			
	M^4	M^0	M^{chem}	M^{scal}
R_1	–	6.2[a]	7.7[b]	5.7
R_2	–	14.3[a]	23.5[b]	14.2
R_3	–	26.2[a]	47.8[b]	26.2
R_4	–	43.3[a]	72.0[b]	42.2
R_5	–	60.2[a]	86.9[b]	61.2
R_6	–	78.8[a]	94.8[b]	79.7
R_7	–	92.2[a]	98.3[b]	92.8
R_8	–	98.6[a]	99.5[b]	97.3

[a]Taken from Ref. [24].
[b]Taken from Ref. [24].

valence-shell configurations. For comparison, we also present the rearrangement probabilities obtained by means of the statistical scaling procedure. In this procedure the partial widths are assumed to be proportional to the number of electrons in a given shell available for radiative or nonradiative transitions (for details see Refs. [54,67]).

For a fully ionized outer shell (M^4), the rearrangement processes are completely suppressed due to the lack of the M-shell electrons which can participate in the L-shell rearrangement transitions. A fully ionized valence configuration corresponds to a situation in which the strong M-shell ionization and/or nanoplasma processes dominate the chemical effect. Rearrangement probabilities reach the highest values for the enriched valence electron fractions formed due to the chemical effect (see the M^{chem} column of Table III). This configuration corresponds to the process in which the electron enrichment of the valence-shell prevails over all other processes which reduce the number of M-shell electrons. Significantly smaller rearrangement probabilities obtained for the unaffected valence-shell configuration (M^0) can be attributed to the balance between the processes which enrich the M-shell and those which are responsible for the reduction in the number of the M-shell electrons (the free-atomic valence configuration). One can also see that the rearrangement probabilities calculated by applying the scaling procedure (see the M^{scal} column of Table III) are close to those obtained by Hartmann for the free atomic valence configuration [24] (see the M^0 column of Table III).

In Fig. 5 the rearrangement probabilities and other rearrangement parameters obtained in the "chemical" procedure are compared with the values obtained by the statistical scaling procedure [33,39,54]. All rearrangement parameters obtained by means of the scaling method significantly differ from those obtained as a result of the calculations that take into account the strong chemical effect. The same is true for the natural widths

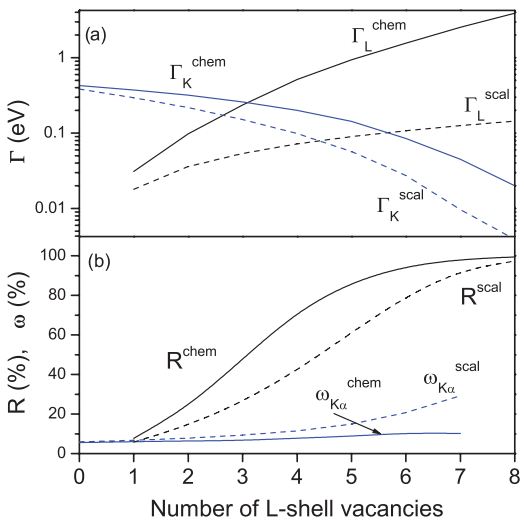

FIG. 5. (Color online) (a) Total K-shell and LMM Auger widths and (b) partial $\omega_{K\alpha}$ fluorescence yields and rearrangement factors for the KL^N ionized states of a Si atom obtained by both scaling (dashed lines) and a procedure taking into account its chemical environment (solid line), respectively. The values obtained by the latter were calculated using the decay rates taken from Ref. [24].

[see Fig. 5(a)]. Moreover, the differences can be dramatically high for states having many L-shell vacancies. In this case the rearrangement processes can gain the extreme high intensity [see the R^{chem} curve in Fig. 5(b)] due to the cascade deexcitation, mainly via the nonradiative LMM Auger transitions [24] [see the Γ_L^{chem} curve in Fig. 5(a)]. This rearrangement cascade dramatically reduces the observed intensities of the high-order $K\alpha L^N$ satellites in the x-ray spectra.

Once the $K\alpha L^N$ satellite intensities and rearrangement factors are known, it is possible to determine the primary L-shell vacancy distributions present at the moment of the ion-atom collision. The primary distributions presented in Sec. IV were obtained from the experimental $K\alpha L^N$ satellite intensities by means of the minimizing fitting procedure, taking into account the rearrangement transformation.

IV. RESULTS AND DISCUSSION

A. Energies of $K\alpha L^N$ satellites

The measured values of the average energy shifts for the $K\alpha L^N$ satellites with respect to the $K\alpha$ diagram lines of Si situated in the chemical oxygen environment (SiO_2) in different stages of the stopping process are listed in Table IV. Figure 6 compares the experimental energy shifts measured for three different energies of the Ca ions slowing down in the aerogel target with the theoretical energy shifts of the $K\alpha L^N$ satellites. The experimental values are significantly lower than those obtained by means of the MCDF calculations for a fully ionized M shell (see the solid line in Fig. 6). Moreover, calculations for the M^0 ($3s^2 3p^2$) valence shell configuration (dotted line in Fig. 6) also slightly overestimate the measured energy shifts.

The disagreement between the experiment and these MCDF calculations seems to increase with the number of the L-shell holes. A similar effect of decreasing energy shifts with the number of the L-shell vacancies has been observed for the fluorine $K\alpha$ x-ray satellites [60]. In that article O. Benka and coauthors interpret this effect as a result of the presence of the additional three to four $3p$ electrons. Afterward, this uniform picture has been re-formed into a more sophisticated theory by Hartman [62]. In this theory the M-subshell fractions depend on the number of the L-shell holes.

The comparison between our experimental and theoretical results disproves the theoretical description based on the uniform effective valence charge picture. It also confirms the

TABLE IV. The average energy shifts of the $K\alpha L^N$ satellites (with respect to the $K\alpha L^0$ diagram lines) measured (in eV) in different stages of the stopping process and different energy ranges of the projectiles interacting with the low-density SiO_2 target.

Satellite type	Ca-ion energy (MeV/u)		
	(11.4–10.6)	(8.5–7.6)	(5.2–4.0)
$K\alpha L^1$	10.1 ± 1.1	9.9 ± 0.9	9.7 ± 1.0
$K\alpha L^2$	22.2 ± 1.2	22.2 ± 0.8	22.7 ± 0.9
$K\alpha L^3$	36.1 ± 1.0	35.6 ± 0.9	36.2 ± 1.0
$K\alpha L^4$	49.6 ± 1.0	50.1 ± 1.0	50.9 ± 1.2
$K\alpha L^5$	63.3 ± 1.2	64.8 ± 1.2	64.8 ± 1.6

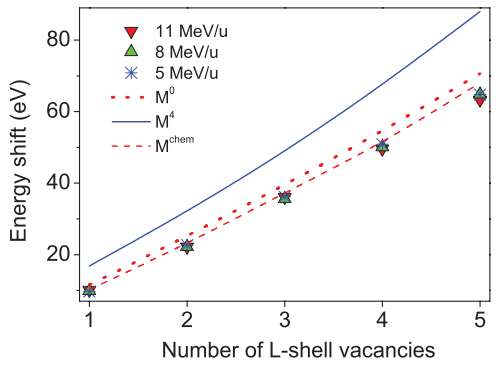

FIG. 6. (Color online) Comparison of the experimental $K\alpha L^N$ satellites energy shifts obtained in the present work for three different Ca-projectile energies: ~11 MeV/u, ~8 MeV/u, and ~5 MeV/u, respectively, with MCDF predictions performed for various valence configurations. The dotted line represents the calculations with full valence shell (M^0), the solid line represents the calculations with a fully ionized one (M^4), and the dashed line corresponds to the a chemical enriched valence configuration (M^{chem}).

correctness of Hartman's approach, in which an increase of the valence electron fraction is strongly related to the number of the L-shell vacancies and chemical environment. Our theoretical calculations of the $K\alpha L^N$ satellite energy shifts with the uniform effective valence charge (M^0 and M^4) do not take into consideration the chemical environment of a Si atom. This is a plausible reason for the observed discrepancies between the experiment and the theory based on the uniform effective valence charge picture.

The MCDF calculations for the valence-electron-rich SiO_2 compound must go beyond the description based on the uniform effective valence charge. Using the enriched valence electron fraction in the theoretical calculations, one can further reduce the values of the calculated $K\alpha L^N$ satellite energy shifts (the dashed line in Fig. 6). An agreement between these theoretical calculations and the experimental values strongly suggests that the valence-shell present at the moment of the $K\alpha$ x-ray transitions is strongly enriched by electrons in all considered phases of the stopping process.

Furthermore, the negligible differences in the energy shifts of every $K\alpha L^N$ satellite observed for different ion penetration depths and therefore different projectile charge and energies indicate that the valence configuration reveals striking similarities in all the stages of the stopping process. At first sight this observation seems to be in a contradiction with the SCA theory that predicts changes in the M-shell configuration due to the increase in the ionization probabilities from $p_M = 0.18$ (per electron for the near central collisions) in the early stage of the stopping process ($E_p \sim 11$ MeV/u) up to $p_M = 0.41$ in the latter ($E_p \sim 5$ MeV/u). A higher M-shell ionization should increase the $K\alpha L^N$ satellite energy shifts, especially at the lowest projectile energy.

On the other hand, a Si atom highly ionized in the inner shells constitutes a large positive charge center in the SiO_2 multiple-valence-electron system with the central force strongly attracting electrons not only from the self-valence (bonding) state but also from the valence states of the neighboring oxygen atoms. This leads to a transformation of the Si valence state and formation of the enriched valence (mainly $3p$ and $3d$) electron fractions. The low values of the experimental energy shifts indicate that in the case of multiple ionized Si situated in the oxygen chemical environment, the valence electron enhancement significantly predominates over the outer-shell ionization.

TABLE V. The $K\alpha L^0$ diagram (X^0) and $K\alpha L^N$ satellite intensities (X^N) measured for different stages of the stopping process and different energy ranges of the projectiles interacting in the low-density SiO_2 target (given in %).

$K\alpha L^N$ line intensities	Ca-ion energy (MeV/u)		
	(11.4–10.6)	(8.5–7.6)	(5.2–4.0)
X^0	14.1 ± 1.4	13.9 ± 1.4	7.3 ± 0.9
X^1	14.6 ± 1.8	13.9 ± 1.6	7.1 ± 1.0
X^2	25.6 ± 1.6	23.2 ± 1.5	20.3 ± 2.2
X^3	22.0 ± 1.9	24.1 ± 1.9	27.6 ± 2.9
X^4	14.8 ± 2.0	14.5 ± 1.9	20.9 ± 2.3
X^5	6.6 ± 1.8	7.8 ± 1.5	11.8 ± 1.6
X^6	2.2 ± 2.0	2.6 ± 2.0	4.9 ± 1.0

B. L-shell vacancy distributions

The relative intensities of the $K\alpha L^0$ diagram and $K\alpha L^N$ satellite transitions of Si induced in the SiO_2 target by the decelerating Ca ions (with initial energy of 11.4 MeV/u) are listed in Table V. The intensities of the $K\alpha L^N$ ($N = 1,2,\ldots,5$) satellite transitions reflect the primary L-shell vacancy distribution arising at different stages of the stopping process. Assuming that the L-shell vacancies can be produced independently in the direct ionization and/or in the electron-capture processes, in the statistical model [see Eqs. (6) and (7)] both processes responsible for the L-shell vacancy production can be described by binomial distributions with free (ionization) and fixed (electron capture) probabilities. In this way, the model distribution [Eq. (8)] fitted to the $K\alpha L^N$ satellite intensities and corrected for the rearrangement processes reproduces the primary L-shell vacancy distribution and the L-shell ionization probabilities. The only free fitting parameter in that procedure is the average L-shell ionization probability per electron p_L, while the electron-capture probability estimated from the eikonal theory is kept fixed. As we have mentioned before, in order to determine the primary L-shell distribution and p_L values, we have excluded the $K\alpha L^0$ x-ray transitions from the $K\alpha L^N$ intensity analysis due to their different origins (secondary photo- and electron-ionization [56]).

The rearrangement parameters governing the primary L-shell distribution strongly depend on the valence-shell configuration. This dependence can be seen in Fig. 7, where the primary L-shell distributions obtained for different assumptions concerning valence shell configurations are displayed. These results represent the distributions for the latest stage of the stopping process, where the highest degree of the L-shell ionization and the most intense rearrangement transitions are expected. The dashed line corresponds to the primary L-shell distribution obtained with assumption of a fully ionized M shell (M^4). In this case rearrangement processes cannot take place because of the lack of electrons in the M shell.

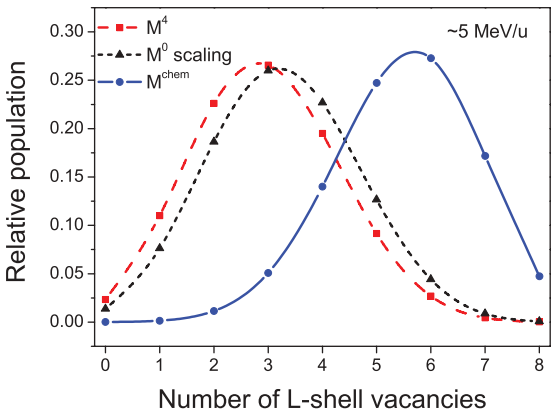

FIG. 7. (Color online) Primary L-shell distributions in Si induced by the Ca ions at $E \sim 5$ MeV/u obtained for different Si valence configurations. The solid line represents the distribution obtained for a chemically enriched valence shell, the dashed line represents the distribution obtained for a fully ionized one (M^4), and the dotted line corresponds to the distribution obtained by means of the scaling procedure (M^0).

Therefore, these results correspond to the unaffected L-shell vacancy distribution observed in the $K\alpha$ x-ray spectra.

In comparison with the M^4 results, the scaling rearrangement procedure (M^0) slightly shifts the L-shell primary distribution toward the higher ionized states (the dotted lines in Fig. 7). The statistical scaling rearrangement approach does not take into consideration the interatomic valence-electron flow from ligands into the ionized Si, which is especially strong in the valence-electron-rich compounds like SiO_2. As a consequence, the valence-electron fraction of the highly ionized Si is under-represented in this approach and the high degree of the L-shell ionization cannot be reproduced.

Finally, the solid line in Fig. 7 represents the primary L-shell distribution obtained by means of the rearrangement procedure taking into consideration the chemical or solid-state enrichment of the valence shell. The primary distribution obtained after the "chemical" rearrangement corrections represents the highest degree of the L-shell ionization present in the later stage of the stopping process.

The proper choice of the rearrangement profile for the considered atomic system embedded in a given chemical environment requires precise knowledge of the valence-shell configuration for each KL^N vacancy state produced in the ion-atom collision. This information can be derived from the experimental energy shifts of the $K\alpha L^N$ satellites which depend on the valence-shell configuration. As argued in previous section, the low values of the $K\alpha L^N$ satellite energy shifts observed in the experiment firmly indicate that in the case of the SiO_2 compound the valence-shell of the multiple ionized Si is significantly enriched by additional electrons. Therefore, we conclude that the chemical rearrangement procedure reproduces the L-shell primary distributions best.

The valence-electron-rich configuration has different consequences for the subsequent rearrangement processes and then for the observed $K\alpha$ x-ray spectra. The results of Hartmann's calculations [24] have shown that any inner-shell Si charge depletion is compensated by a corresponding increase of the Si $3s$, $3p$, and $3d$ electron charge fraction. The valence configuration of Si situated in SiO_2 chemical compound can evolve from $\sim 3s^2 3p^2 3d^1$ for the KL^1 state into $\sim 3s^2 3p^5 3d^4$ for the KL^7 one. In other words, the inner-shell charge depletion related with L-shell ionization of the Si atom initiates a very intense valence electron flow from the oxygen ligands.

Moreover, even the $3s$ or $3p$ outer-shell ionization and/or rearrangement processes can be easily compensated by the $3d$ electron charge fraction. Both electron compensations increase dramatically for the high degree of the L-shell ionization and "prepare" the Si atom for the subsequent cascade deexcitation. This valence electron enhancement of Si situated in the electron-rich chemical environment is manifested by a huge increase in the deexcitation rates for the L-shell rearrangement transitions occurring from the valence shell prior to the $K\alpha$ x-ray emission. Such extreme atomic conditions induce cascade rearrangement processes occurring mainly by LMM (LVV) Auger transitions. The decay rates of the LMM transitions increase from the $\sim 5 \times 10^{13}$ s^{-1} for the KL^1 state up to $\sim 4 \times 10^{15}$ s^{-1} for the KL^7 one [24]. One of the reasons for such huge rearrangement intensities for highly ionized states is the growing role of Si $3d$ electrons in the L-shell vacancy filling through the LMM cascade transitions.

By the comparison with decay rates of $K\alpha L^N$ satellites ranging from $\sim 7 \times 10^{12}$ s^{-1} ($K\alpha L^7$) up to $\sim 3 \times 10^{13}$ s^{-1} ($K\alpha L^1$), one can clearly see that the LMM cascade processes are sufficiently intense to fill the L-shell vacancies prior x-ray emission. In this way, the fast rearrangement processes transform the highly ionized KL^N states, produced in the ion-atom collisions, into the states with the reduced number of the L-shell vacancies and shift the maximum of the L-shell vacancy distribution toward the lower energy range of the K x-ray spectra.

This L-shell vacancy reduction in all stages of the stopping process is shown in Fig. 8. Here the primary L-shell vacancy distributions are shown together with the distributions present at the moment of the K x-ray emission. The results represent the primary populations of the KL^N vacancy states appearing at the Ca-ion energies of ~ 11 MeV/u, ~ 8 MeV/u, and ~ 5 MeV/u. The highest degree of the L-shell ionization can be seen clearly at the lower Ca-projectile energy of ~ 5 MeV/u. The "chemical" rearrangement processes significantly reduce the primary L-shell vacancy populations of the highest ionized states for all phases of the stopping process. The strongest reduction occurs in the latest stage of the stopping process where the L-shell vacancy production is the most intense. At this stage the strong rearrangement transitions efficiently reduce the number of the highest ionized states. A similar effect of the high efficiency in reduction of the L-shell vacancies prior to the K x-ray emission has been observed in the previous experimental works concerning low-Z atoms in the electron-rich chemical (or solid-state) surroundings [58,68].

C. L-shell vacancy-production probabilities

The experimental and theoretical L-shell ionization probabilities for the Si atoms induced by the Ca ions obtained from fitting the model distribution [Eq. (8)] to the $K\alpha L^N$ satellite intensities are shown in Table VI. The theoretical values were obtained by means of the SCA and geometrical model (GM) [69] approximations, respectively. For completeness the

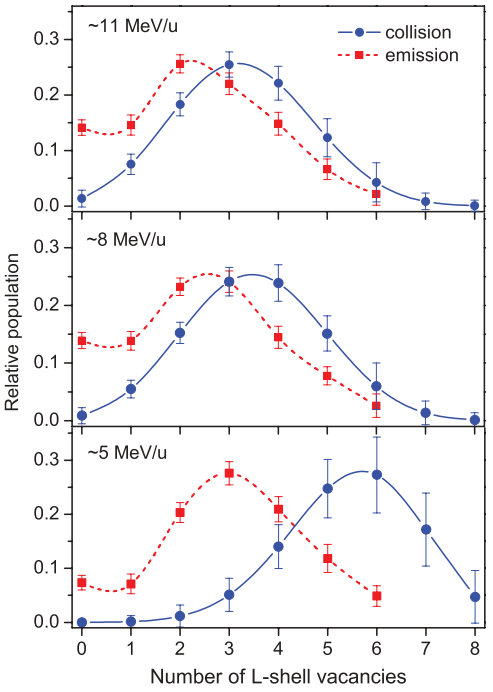

FIG. 8. (Color online) The $K\alpha L^N$ satellite intensities (squares and dashed lines) measured in the $K\alpha$ x-ray spectra induced in Si by the Ca ions with initial energy of 11 MeV/u at early (top), mid- (middle), and later stages of the stopping processes (bottom) and corresponding primary L-shell vacancy distributions (circles and solid lines) obtained by means of the "chemical" rearrangement procedure.

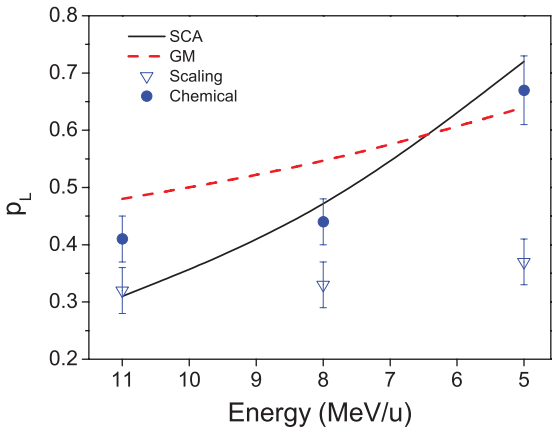

FIG. 9. (Color online) Comparison of the experimental L-shell ionization probabilities for Si atoms (per electron) exited by the Ca ions at different stages of the stopping processes with the predictions of the SCA-HYD and GM theoretical calculations as a function of the projectile energy (in reverse scale). The triangles and circles represent the experimental values obtained by scaling and "chemical" rearrangement procedures, respectively.

probabilities of the electron capture from L-shell of the target atom into bound states of projectile estimated from the eikonal capture cross sections [55] and used in the fitting procedure are also presented.

Due to a very small contribution of the electron-capture processes to the total L-shell vacancy production, we believe that the fitting procedure (with fixed electron-capture probabilities) accurately reproduces the average L-shell ionization probabilities for all considered stages of the stopping process. In the case of the later phase, the cross sections of the electron capture significantly increases. This can lead to a higher contribution of the electron-capture processes to the L-shell vacancy production. To the best of our knowledge there are no impact-parameter-dependent studies devoted to the $L \rightarrow M,N$ electron-capture processes occurring in the strong perturbation regime considered in our work. Therefore, we point out that in the case of the later stage (~5 MeV/u) the systematic error of the L-shell ionization probability can be slightly higher than those for the early and mid stages.

The values of the L-shell ionization probabilities obtained from different rearrangement procedures that transform the $K\alpha L^N$ satellite intensities into the primary L-shell distribution (or vice versa) can significantly differ from each other. The results obtained by means of the simplified scaling rearrangement procedure are displayed in the next-to-last column of Table VI [$(p_L^{\mathrm{DI}})_{\mathrm{scal}}$]. The experimental values obtained after the correction taking into account the rearrangement enhancement due to the electron-rich chemical environment of a Si atom (SiO_2) are shown in the last column of Table VI [$(p_L^{\mathrm{DI}})_{\mathrm{chem}}$]. Figure 9 illustrates the direct ionization probabilities obtained by both rearrangement procedures as well as the SCA and GM theoretical predications.

One can see that the direct L-shell ionization probabilities determined by means of the chemical rearrangement procedure are significantly higher than those obtained by means of the scaling method. Moreover, the scaling procedure is not able to reproduce the strong dependence between the L-shell ionization probabilities and the projectile energies that is

TABLE VI. The theoretical (SCA and GM) and experimental L-shell ionization probabilities for Si atoms (per electron) induced by the Ca ions obtained by fitting the model distribution [Eq. (8)] to the $K\alpha L^N$ satellite intensities corrected for rearrangement processes. The symbols $(p_L^{\mathrm{DI}})_{\mathrm{scal}}$ and $(p_L^{\mathrm{DI}})_{\mathrm{chem}}$ represent direct ionization probabilities obtained by means of the scaling and "chemical" rearrangement procedure, respectively (for details see text). The theoretical L-shell electron-capture probabilities estimated from the eikonal capture cross sections [55] and used in fitting procedure are also shown.

Projectile energy	Theory			Experiment	
	$(p_L^{\mathrm{EC}})_{\mathrm{eikonal}}$	$(p_L^{\mathrm{DI}})_{\mathrm{GM}}$	$(p_L^{\mathrm{DI}})_{\mathrm{SCA}}$	$(p_L^{\mathrm{DI}})_{\mathrm{scal}}$	$(p_L^{\mathrm{DI}})_{\mathrm{chem}}$
~11 MeV/u	0.002	0.48	0.31	0.32 ± 0.04	0.41 ± 0.04
~8 MeV/u	0.008	0.54	0.45	0.33 ± 0.04	0.44 ± 0.04
~5 MeV/u	0.074	0.64	0.72	0.37 ± 0.04	0.67 ± 0.05

predicted by both SCA and GM theories (see Fig. 9). These striking differences between the values of the direct L-shell ionization probabilities obtained after the scaling and chemical rearrangement corrections are related to the fact that the scaling procedure significantly underestimates the rearrangement processes occurring in the highly ionized Si atoms situated in the chemical and/or nanoplasma environment. In this way the scaling procedure reproduces the primary L-shell distribution anomalously shifted toward the lower number of the L-shell vacancies. As a consequence, the obtained values of the L-shell ionization probabilities are artificially understated.

In contrast to that, the chemical rearrangement procedure that takes into account the enhanced rearrangement processes occurring in the electron-rich environment of the SiO_2 compound reliably reproduces the high degree of the L-shell ionization at the moment of the ion-atom collision. As a result, the values of the direct L-shell ionization probabilities are much higher than those obtained by means of the scaling procedure. This finding once more confirms the great importance of the chemical (solid-state) approach to the rearrangement processes, which modify the valence-shell configuration of the highly ionized atomic systems.

D. Nanosize plasma effects

Lankin *et al.* [44] have proposed a relaxation model of low-temperature plasma (10–50 eV) generated by a fast single ion in condensed matter. This collisional-radiative model predicts the time-dependent population of the Si ground and excited states produced in the track due to collisions with the plasma electrons. The model is based on the assumption that the plasma structures are localized inside the ion track core. Further assumptions concern the Maxwell distribution of the plasma electrons, the constant values of the plasma electron density and temperature during the x-ray irradiation and finally the fully ionized M-shell after the direct interaction with a projectile.

Although this is not the only factor affecting the post-collisional rearrangement, a solid-density plasma appearing in the ion track can affect the relative intensities of the $K\alpha L^N$ satellite lines, which in "pure" atomic conditions are the signature of the primary distributions of the KL^N states induced in the ion-atom collisions. In the model it is assumed that the solid-density nanosize plasma in the area of the ion track is uniformly created. In our analysis of the spectra measured at the different projectile energies, the only symptom of the plasma nanofields inside the ion track is related to the increase in the broadening of the $K\alpha L^N$ lines. In the case of the $K\alpha L^1$ satellite structure, the total width increased from $\sim$4 eV up to $\sim$6 eV in the spectra emitted at the early and later stages of the stopping process, respectively.

In the plasma relaxation model it has also been assumed that the free electrons and the highly ionized states of the target atoms (ions) with a single K-shell vacancy, the N number of the L-shell vacancies, and the fully ionized M-shell are produced in the area of the projectile-target atom interaction. The part of this assumption related to the fully ionized M shell is an obvious contradiction with the binary-encounter estimations and results obtained in the experiment. The values of the experimental $K\alpha L^N$ satellite energy shifts reflect the strong M-shell electron enrichment at the moment of x-ray emission. The nanoplasma effects can also contribute to the reduction of the $K\alpha L^N$ transition energies (the so-called red shift) caused by the electron gas pressure in the track core [45,46]. However, even the strong nanoplasma effects cannot reduce the energy of the $K\alpha$ satellite transitions to the values observed in our experiment. For example, in the case of the $K\alpha L^4$ satellite the energy of the x-ray transition in Si can be reduced by only 1–8 eV in a plasma environment with electron density ranges from 1×10^{23} up to 5×10^{23} cm^{-3} and electron temperature from 10 eV up to 50 eV [70]. Meanwhile, the energies of the $K\alpha L^4$ satellites observed in the experiment are reduced by more than 16 eV in comparison with the corresponding energies of the $K\alpha L^4$ satellite transitions occurring in the presence of a fully ionized M shell.

Furthermore, if the electron gas pressure was the only factor responsible for the reduction of satellite transition energy, the values of the energy shifts should increase with the ion penetration depth, especially at the lowest projectile energies due to the increase in the density and the temperature of the ionized target electrons. It should be noted that the experimental values of the energy shift for every $K\alpha L^N$ satellite group does not depend on the ion penetration depth and thus on the ion charge and velocity. Finally, the reduced number of the L-shell vacancies observed in the $K\alpha L^N$ satellite spectra proves the extremely strong rearrangement processes related with $M \rightarrow L$ electron transitions. These transitions cannot occur when the M-shell is entirely empty. In our view, this eventually proves that the M shell is strongly enriched at the moment of the x-ray emission and the plasma effect might play at most a secondary role in the reduction of the K-shell x-ray transitions induced in the stopping media during the considered phases of the stopping process.

The electron enhancement of the valence shell observed at the moment of the x-ray radiation induced by the projectiles with energies $\sim$5 MeV/u and above suggests a neutralization of the ion track core potential in the femtosecond time scale after ionization by projectile ions. This indicates that the Coulomb explosion and the following material deformation are prevented in the early and intermediate phases of the stopping process.

Another conclusion presented by Lankin [44] concerns the phase of the nanoplasma relaxation that significantly contributes to the x-ray emission. It has been shown that the most intensive spectral lines are radiated during the first 7 fs after the projectile-target atom interaction. The calculations of the atomic decay rates for Si with the electron-enriched M shell predict lifetimes of the KL^N states from 1.5 fs (for KL^0) up to 14.6 fs (for KL^7), which is in an agreement with the values obtained in the plasma relaxation model.

Finally, we comment on the L-shell ionization probabilities obtained from the fitting of the plasma parameters to the experimental spectra [44]. The weak dependence between the L-shell ionization probabilities and the projectile energies is a further consequence of the fully ionized M shell assumed in the plasma relaxation model. Based on this assumption, the rearrangement processes cannot be included in the calculations. In this way, the highest ionized KL^N states are under-represented in the model, especially as far as the later phases of the stopping process are concerned. Similarly, an inadequate scaling rearrangement procedure applied in

our analysis of the $K\alpha L^N$ satellite intensities resulted in a weak dependence between the L-shell ionization probabilities and the projectile energies (for details, see the previous section).

V. SUMMARY AND CONCLUSIONS

The $K\alpha$ x-ray spectra of Si induced by the 11.4 MeV/u Ca projectile slowing down in the low-density aerogel SiO_2 target have been studied for different stages of the ion-stopping process. The measurements with a high-energy resolution (comparable with the natural line width) provided precise experimental data concerning the intensities and energies of the $K\alpha L^N$ x-ray satellite transitions occurring in a Si atom situated in the valence-electron-rich chemical environment.

It was found that the energy shifts of the $K\alpha L^N$ satellites measured with respect to the $K\alpha$ diagram lines do not depend on the Ca projectile energy. The low-energy shifts of the $K\alpha L^N$ satellites observed in the experiment were attributed to the chemical effect that decreases the $K\alpha L^N$ satellite transition energies due to the enrichment of the valence-electron fraction. Furthermore, it was demonstrated that this effect is prominent for higher-order $K\alpha L^N$ satellites where the L shell of a Si atom is highly ionized. It was also shown that the nanoplasma effects in the area of the ion track can play only a secondary role in the reduction of the $K\alpha L^N$ satellite energy shifts (the red shift) in early and intermediate phases of the stopping process. For those phases the assumption of the nanoplasma relaxation model concerning the fully ionized M shell seems to be unjustified.

The L-shell vacancy distributions of Si at the moment of the ion-atom collisions occurring in different phases of the stopping process were obtained from fitting the model distribution into the measured $K\alpha L^N$ satellite intensities corrected for the rearrangement processes. Our results show a high level of the L-shell ionization during all considered phases of the stopping process. The L-shell vacancy production is especially intense in the later phase of the stopping process, when the probability of the L-shell ionization reaches almost 70%.

The populations of the highly ionized KL^N states appearing in the Si atoms after the interaction with the Ca ions were found to undergo a significant reduction in the time between the ion-atom collision and the x-ray emission due to the very intense rearrangement processes. This reduction is especially striking for the latest (considered in this work) phase of the stopping process, where a degree of the L-shell ionization is expected to be the highest. As a consequence, the highest ionized states of Si produced in the ion-atom collisions cannot be directly observed in the $K\alpha$ satellite x-ray spectra. The high intensity of the rearrangement processes was attributed to the electron-rich chemical environment which modifies the valence shell of Si being in the highly ionized KL^N states. The importance of the chemical approach for the rearrangement processes was also shown in the procedures used in order to determine the L-shell ionization probabilities.

ACKNOWLEDGMENTS

Partial support for this work was provided by the Polish Ministry of Science and Higher Education under Grant No. N N202 1465 33. We also thank Doris Jakubassa for the K-K and L-K electron-capture probability calculations, as well as Jean-Claude Dousse and Joanna Hoszowska for carrying out the x-ray measurements of the $K\alpha L^0$ chemical shift in the SiO_2 low-density aerogel. We appreciate Siegbert Hartmann, Vladimir Efremov, and Alexander Volkov's fruitful contribution to the discussion. We are also very grateful to Viatcheslav Shevelko for the cross-section calculations.

[1] J. R. Mowat, I. A. Sellin, D. J. Pegg, R. S. Peterson, M. D. Brown, and J. R. Macdonald, Phys. Rev. Lett. **30**, 1289 (1973).
[2] A. R. Knudson, P. G. Burkhalter, and D. J. Nagel, Phys. Rev. A **10**, 2118 (1974).
[3] J. R. Mowat, I. A. Sellin, P. M. Griffin, D. J. Pegg, and R. S. Peterson, Phys. Rev. A **9**, 644 (1974).
[4] R. L. Kauffman, K. A. Jamison, T. J. Gray, and P. Richard, Phys. Rev. Lett. **36**, 1074 (1976).
[5] C. Schmiedekamp, B. L. Doyle, T. J. Gray, R. K. Gardner, K. A. Jamison, and P. Richard, Phys. Rev. A **18**, 1892 (1978).
[6] H. F. Beyer, R. Mann, F. Folkmann, and P. H. Mokler, J. Phys. B **15**, 3853 (1982).
[7] P. Sigmund, *Stopping of Heavy Ions*, Springer Tracts of Modern Physics No. 204 (Springer, Berlin, 2004).
[8] F. F. Komarov, Phys. Usp. **46**, 1253 (2003).
[9] R. Kelly and M. Fernanda (eds.), *Materials Modification by High-Fluence Ion Beams* (Kluwer Academic, New York, 1989).
[10] D. H. H. Hoffmann *et al.*, Laser Part. Beams **23**, 47 (2005).
[11] J. J. MacFarlane, P. Wang, J. Bailey, T. A. Mehlhorn, R. J. Dukart, and R. C. Mancini, Phys. Rev. E **47**, 2748 (1993).
[12] G. Kraft, Prog. Part. Nucl. Phys. **45**, S473 (2000).
[13] G. Schiwietz, E. Luderer, G. Xiao, and P. L. Grande, Nucl. Instrum. Methods Phys. Res. B **175-177**, 1 (2001).
[14] G. Schiwietz, K. Czerski, M. Roth, F. Staufenbiel, and P. L. Grande, Nucl. Instrum. Methods Phys. Res. B **226**, 683 (2004).
[15] R. L. Fleischer, P. B. Price, R. M. Walker, and E. L. Hubbard, Phys. Rev. **156**, 353 (1967).
[16] E. M. Bringa and R. E. Johnson, Phys. Rev. Lett. **88**, 165501 (2002).
[17] C. Trautmann, S. Klaumünzer, and H. Trinkaus, Phys. Rev. Lett. **85**, 3648 (2000).
[18] O. N. Rosmej *et al.*, Nucl. Instrum. Methods Phys. Res. A **495**, 29 (2002).
[19] O. N. Rosmej *et al.*, Rev. Sci. Instrum. **74**, 5039 (2003).
[20] O. N. Rosmej *et al.*, Phys. Rev. A **72**, 052901 (2005).
[21] S. A. Pikuz Jr., V. P. Efremov, O. Rosmej, A. Blazevic, S. Korostiy, A. Fertman, A. V Shutov, H. E. Norman, and D. H. H. Hofmann, J. Phys. A **39**, 4765 (2006).
[22] V. P. Shevelko, Tech. Phys. **46**, 1225 (2001).
[23] S. Eisenbarth, O. N. Rosmej, V. P. Shevelko, A. Blazevic, and D. H. H. Hoffman, Laser Part. Beams **25**, 601 (2007).
[24] E. Hartmann, J. Phys. B **20**, 475 (1987).
[25] P. L. Grande and G. Schiwietz, Phys. Rev. A **47**, 1119 (1993).

[26] N. G. Borisenko and Ya. A. Merkuliev, in *Proceedings of P. N. Lebedev Institute* (Nova Science Publishers, New York, 1996), Vol. 221.
[27] B. A. Demidov, V. P. Efremov, M. V. Ivkin, I. A. Ivonin, V. A. Petrov, and V. E. Fortov, Zh. Tekh. Fiz. **43**, 1239 (1998).
[28] A. Fertman *et al.*, Europhys. Conf. Abstr. **30**(I), 2.001 (2006).
[29] A. Ya. Faenov, S. A. Pikuz Jr., A. I. Erko, B. A. Bryunetkin, V. M. Dyakin, G. V. Ivanenkov, A. R. Mingaleev, T. A. Pikuz, V. M. Romanova, and T. A. Shelkovenko, Phys. Scr. **50**, 333 (1994).
[30] B. L. Henke and P. A. Jaanimagi, Rev. Sci. Instrum. **56**, 1537 (1985).
[31] V. Horvat, R. L. Watson, and Y. Peng, Phys. Rev. A **74**, 022718 (2006).
[32] J. Rzadkiewicz, O. Rosmej, A. Blazevic, V. P. Efremov, A. Gójska, D. H. H. Hoffmann, S. Korostiy, M. Polasik, K. Słabkowska, and A. E. Volkov, High Energy Density Phys. **3**, 233 (2007).
[33] J. Rzadkiewicz *et al.*, Phys. Rev. A **68**, 032713 (2003).
[34] K. Słabkowska and M. Polasik, J. Phys. Conf. Ser. **163**, 012040 (2009).
[35] J. L. Campbell and T. Papp, At. Data Nucl. Data Tables **77**, 1 (2001).
[36] G. Graeffe, H. Juslén, and M. Karras, J. Phys. B **10**, 3219 (1977).
[37] J. A. Tossell, Geochim. Cosmochim. Acta **37**, 583 (1973).
[38] M. Polasik, Phys. Rev. A **52**, 227 (1995).
[39] M. Kavčić *et al.*, Phys. Rev. A **61**, 052711 (2000).
[40] Z. Liu, S. Sugata, K. Yuge, M. Nagasono, K. Tanaka, and J. Kawai, Phys. Rev. B **69**, 035106 (2004).
[41] T. Okura, H. Inoue, T. Kanazawa, S. Endo, S. Fukushima, and Y. Gohshi, Spectrochim. Acta Part B **45**, 711 (1990).
[42] J. Hoszowska, J-Cl. Dousse, A. Gójska, J. Rzadkiewicz, and K. Słabkowska (unpublished).
[43] J. Hoszowska, J.-Cl. Dousse, J. Kern, and Ch. Rhême, Nucl. Instrum. Methods A **376**, 129 (1996).
[44] A. V. Lankin, I. V. Morozov, G. E. Norman, S. A. Pikuz Jr., and I. Yu. Skobelev, Phys. Rev. E **79**, 036407 (2009).
[45] S. Skupsky, Phys. Rev. A **21**, 1316 (1980).
[46] H. Nguyen, M. Koenig, D. Benredjem, M. Caby, and G. Coulaud, Phys. Rev. A **33**, 1279 (1986).
[47] N. A. Medvedev and A. E. Volkov, AIP Conf. Proc. **999**, 238 (2008).
[48] R. L. Kauffman, J. H. McGuire, P. Richard, and C. F. Moore, Phys. Rev. A **8**, 1233 (1973).
[49] R. L. Watson, F. E. Jenson, and T. Chiao, Phys. Rev. A **10**, 1230 (1974).
[50] D. Trautmann, F. Rösel, and G. Baur, Nucl. Instrum. Methods Phys. Res. **214**, 21 (1983).
[51] D. Trautmann and F. Rösel, Nucl. Instrum. Methods **169**, 259 (1980).
[52] M. Pajek, A. P. Kobzev, D. Trautmann, and Th. Kauer, Nucl. Instrum. Methods Phys. Res. B **52**, 109 (1990).
[53] D. H. Jakubassa-Amundsen (private communication).
[54] P. Rymuza, Z. Sujkowski, M. Carlen, J.-Cl. Dousse, M. Gasser, J. Kern, B. Perny, and Ch. Rhême, Z. Phys. D **14**, 37 (1989).
[55] J. K. M. Eichler, Phys. Rev. A **23**, 498 (1981).
[56] R. L. Watson, J. M. Blackadar, and V. Horvat, Phys. Rev. A **60**, 2959 (1999).
[57] V. Horvat and R. L. Watson, J. Phys. B **34**, 777 (2001).
[58] R. L. Watson, A. K. Leeper, B. I. Sonobe, T. Chiao, and F. E. Jenson, Phys. Rev. A **15**, 914 (1977).
[59] J. McWherter, D. K. Olsen, H. H. Wolter, and C. F. Moore, Phys. Rev. A **10**, 200 (1974).
[60] O. Benka, R. L. Watson, B. Bandong, and K. Parthasaradhi, Phys. Rev. A **29**, 123 (1984).
[61] J. Hoszowska, J.-Cl. Dousse, D. Castella, D. Corminboeuf, J. Kern, Y.-P. Maillard, and P.-A. Raboud, J. Phys. B **33**, 3165 (2000).
[62] E. Hartmann, J. Phys. B **19**, 1899 (1986).
[63] E. J. McGuire, Phys. Rev. A **3**, 587 (1971).
[64] J. H. Scofield, Phys. Rev. A **9**, 1041 (1974).
[65] E. J. McGuire, Phys. Rev. A **2**, 273 (1970).
[66] V. O. Kostroun, M. H. Chen, and B. Crasemann, Phys. Rev. A **3**, 533 (1971).
[67] F. P. Larkins, J. Phys. B **4**, L29 (1971).
[68] R. L. Watson, T. Chiao, and F. E. Jenson, Phys. Rev. Lett. **35**, 254 (1975).
[69] B. Sulik, I. Kádár, S. Ricz, D. Varga, J. Végh, G. Hock, and D. Berényi, Nucl. Instrum. Methods Phys. Res. B **28**, 509 (1987).
[70] A. Sengebusch (private communication).